Optical and acoustic metamaterials: superlens, negative refractive index and invisibility cloak

2017 J. Opt. 19 084007

(http://iopscience.iop.org/2040-8986/19/8/084007)

J. Opt. 19 (2017) 084007 (13pp) https://doi.org/10.1088/2040-8986/aa7a1f

Optical and acoustic metamaterials: superlens, negative refractive index and invisibility cloak

Zi Jing Wong[1], **Yuan Wang**[1,2], **Kevin O'Brien**[1], **Junsuk Rho**[3,4], **Xiaobo Yin**[5], **Shuang Zhang**[6], **Nicholas Fang**[7], **Ta-Jen Yen**[8] **and Xiang Zhang**[1,2]

[1] NSF Nanoscale Science and Engineering Center, University of California, Berkeley, CA 94720, United States of America
[2] Materials Sciences Division, Lawrence Berkeley National Laboratory, Berkeley, CA 94720, United States of America
[3] Department of Mechanical Engineering, Pohang University of Science and Technology, Pohang 37673, Republic of Korea
[4] Department of Chemical Engineering, Pohang University of Science and Technology, Pohang 37673, Republic of Korea
[5] Department of Mechanical Engineering, University of Colorado, Boulder, CO 80309, United States of America
[6] School of Physics and Astronomy, University of Birmingham, Birmingham B15 2TT, United Kingdom
[7] Department of Mechanical Engineering, Massachusetts Institute of Technology, Cambridge, MA 02139, United States of America
[8] Department of Materials Science and Engineering, National Tsing Hua University, Hsinchu 30013, Taiwan

E-mail: xiang@berkeley.edu

Received 20 December 2016, revised 7 June 2017
Accepted for publication 19 June 2017
Published 21 July 2017

CrossMark

Invited Contribution to the Special Issue 'The History of Metamaterials'.

Abstract

Metamaterials are artificially engineered materials that exhibit novel properties beyond natural materials. By carefully designing the subwavelength unit cell structures, unique effective properties that do not exist in nature can be attained. Our metamaterial research aims to develop new subwavelength structures with unique physics and experimentally demonstrate unprecedented properties. Here we review our research efforts in optical and acoustic metamaterials in the past 15 years which may lead to exciting applications in communications, sensing and imaging.

Keywords: optical metamaterials, acoustic metamaterials, quantum metamaterials

(Some figures may appear in colour only in the online journal)

1. Background

The behaviors of natural materials are known to primarily depend on their chemical constituents, which limits the material properties available for high performance applications. Over the last decade, a new class of engineered materials has emerged, which relies on the structural design of the building blocks, provided the unit cell structure is much smaller than the wavelength of interest. Electromagnetic, acoustic as well as other wave-related properties that are otherwise unattainable in nature can now be realized in these artificially engineered materials, or so-called metamaterials. The beginning of the field of metamaterials is closely linked to the theoretical discovery and experimental pursuit of the negative refractive index medium. Back in 1968, Veselago theoretically showed that negative electric permittivity and negative magnetic permeability could combine to produce a negative refractive index material (NIM) not attainable in nature [1]. While the paper described the highly unusual consequences of the NIM such as negative refraction and reversed Doppler effect, there was no clear recipe on how to construct such an imagined NIM. It was not until three decades later that Pendry and co-authors proposed the ideas of using metallic wires [2] and split-ring resonators (SRRs) [3] to attain negative permittivity and negative permeability, respectively. In addition to providing practical building blocks to realize the NIM, Pendry and co-authors further conceived two unprecedented capabilities of NIMs, i.e. perfect imaging [4] and invisibility cloaking [5], which sparked worldwide metamaterials research. In 2001, Shelby, Smith and Schultz experimentally demonstrated a negative refractive index material at microwave frequencies by integrating metallic wires and SRRs on printed circuit boards [6]. The realization of the NIM not only put an end to the heated debate on the very existence of negative refractive index, but it also demonstrated the possibility of engineering exotic material properties by subwavelength structuring. Despite the early success in realizing metamaterials in the microwave frequency, certain material properties such as the magnetic response can still be found in natural materials in microwave frequency regime. Therefore the quest for unprecedented optical magnetism, NIM and other exotic properties represents an outstanding milestone in physics, which for us began with the Multidisciplinary University Research Initiatives Program in 2000 [7].

2. Optical magnetism and negative refractive index

A material's electric and magnetic responses to the external field are fundamentally different. For electrical excitation, electrons as a monopole can respond very fast resulting in strong optical response of materials and their colorful appearance. Magnetic responses of materials are based on the magnetic dipoles that often form domains which cannot respond fast enough, typically limited to hundreds of GHz range. This dipole nature results in an extremely weak or non-magnetic response of the natural materials at optical frequencies. The search for optical magnetism has lasted for decades but to no success. In 1999, Pendry and co-authors proposed the use of a split-ring structure with dimension much smaller than the wavelength as the building block to attain magnetic response even in non-magnetic parental materials. The structure allows currents to run in a loop and accumulate charges across the gap, which gives rise to a resonance to enhance the magnetic response even at high frequencies [3]. The ability to engineer electromagnetic properties in optical frequency regime is of importance for applications in spectroscopy, imaging, security and communications. In 2004, we set out for the experimental realization of optical magnetism at far-infrared region by microfabricating a layer of planar SRRs consisting of concentric annuli with oppositely facing gaps [8]. At its resonant frequency, magnetic flux penetrating the SRR will induce circular currents and lead to an effective magnetic dipole moment. By performing ellipsometry measurement on our fabricated SRR samples, we observed optical magnetism at far-infrared frequency (figures 1(a) and (b)). We also retrieved these peaks and unveiled the Lorentz-mode-like spectra of magnetic response, showing negative real part of permeability and peaks of imaginary part of permeability near the resonance frequencies. By simply varying the sizes of SRRs, these magnetic resonances can be further tuned, which provides an additional advantage of scalable magnetism to higher frequency that does not exist in natural magnetic materials.

Strong optical magnetism that gives rise to negative permeability is highly sought after, for its combination with the negative permittivity can lead to negative refractive index metamaterials (NIMs) in the optical frequency regime. However, it is challenging to realize negative refractive index at such high frequency range using SRR structures. This is because SRR's resonant frequency scales linearly with its size only up to the mid-infrared range, where the kinetic inductance starts to dominate and weaken the resonance. To extend the saturation frequency towards near-infrared and visible wavelengths, other structures had been used, such as paired nanorods [9] and metal/dielectric/metal fishnet structures [10]. While both works managed to achieve optical negative refractive index, these structures contained a significant amount of loss, which led to low figure of merits (FOMs), defined as the ratio between the real part and the imaginary part of the index. In addition, most of the optical NIMs demonstrated consisted of a single layer of meta-atoms which renders the definition of refractive index difficult, as it is a measure of the bulk property. This class of metamaterials is analogous to a 'gas-phase' material where interactions or coupling between meta-atoms are negligible. Furthermore, negative refraction has not been directly observed in these past NIM experiments.

In 2008, we realized a three-dimensional bulk optical NIM using 21 alternating layers of silver (30 nm) and magnesium fluoride (50 nm) to form a cascaded fishnet structure [11]. Different from the 'gas-phase' metamaterials, this new design exploited the strong coupling between neighboring unit cells, resulting in a 'condensed matter' like properties where the coupling largely determines its collective optical property. The bulk negative refractive index exhibited significantly lower loss than that of 'gas phase' metamaterials, which resulted in a FOM of 3.5. Microscopically, this was due to the antisymmetric current distribution across each metal film, leading to cancellation of the current in the center and therefore a much lower ohmic loss. Subsequently, we carved out a wedge shape on the bulk fishnet NIM (figure 1(c)) and evidently observed optical negative refractive index for wavelengths between 1.55 and 1.75 μm (figure 1(d)). In addition, we also observed optical zero-index at 1.5 μm and positive index of less than one (in vacuum, the smallest in all bulk natural materials) in the range from 1.2 to 1.5 μm.

Despite the unambiguous negative refraction results, the bulk fishnet structure only worked for a particular polarization. We later overcame this problem by using a chess metamaterial formed by squared nanoring structures [12]. By physically shifting the closed nanorings, the symmetric electric and anti-symmetric magnetic resonances can be negatively coupled. The symmetry was broken in such a way to invert the plasmon hybridization and enable the attainment

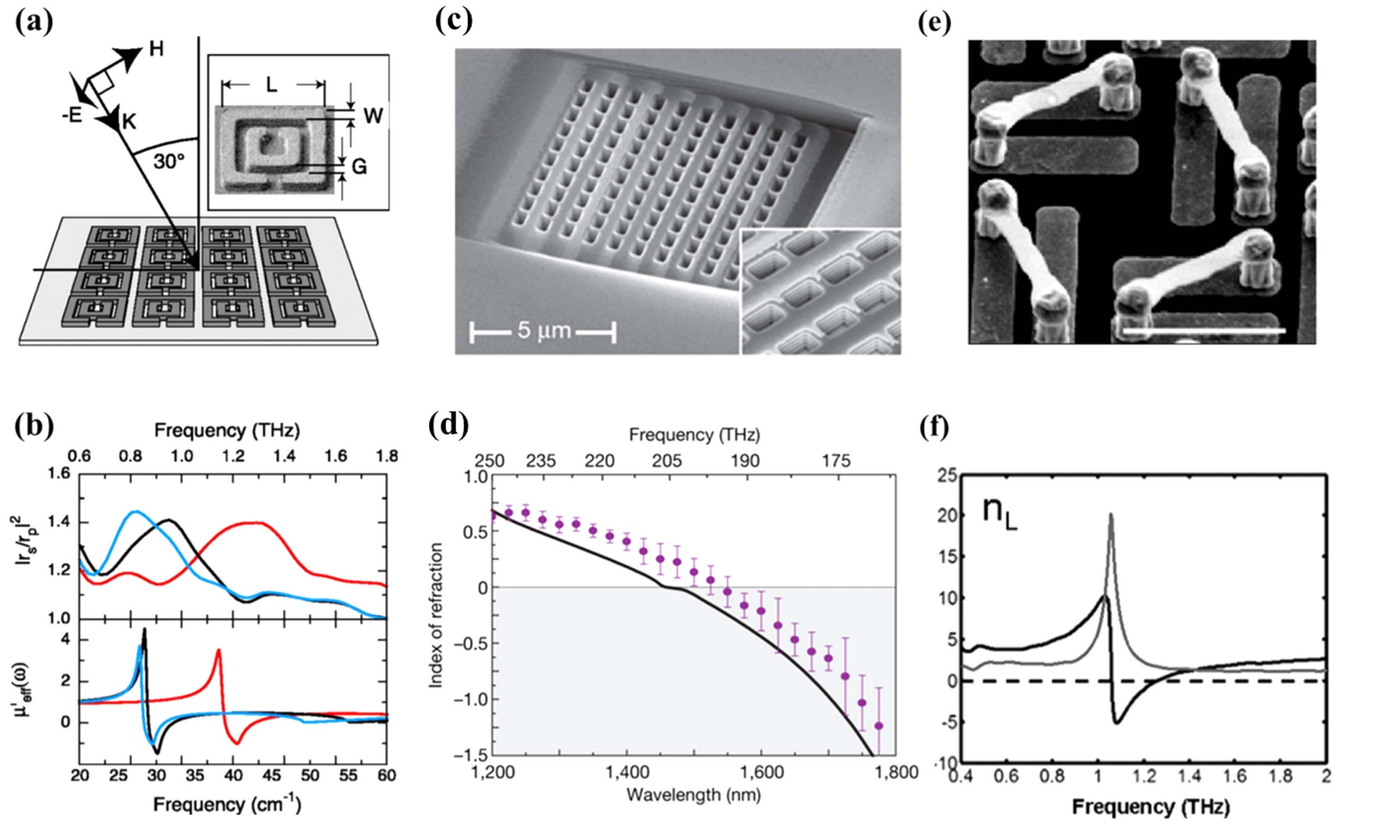

Figure 1. Optical magnetism and negative refractive index. (a) A periodic array of microstructures consisting of double split-ring resonators was fabricated and characterized in a 30° ellipsometry experiment using *s*-polarized beam. (b) The measured ratio of the magnetic to electric response (top) and the simulated real part of the magnetic permeability (bottom) for three different fabricated samples, indicating the attainment of optical magnetic response at far-infrared frequency. (c) SEM image of a NIM prism made from bulk fishnet metamaterials consisting of multilayer stacks of silver and magnesium fluoride with patterned holes. (d) The measured refractive index (circles with error bars) was found to agree closely with the simulated refractive index (black line), where the negative index was evidently demonstrated between 1550 and 1750 nm wavelengths. (e) SEM image of a chiral metamaterial which effective electric and magnetic dipoles sharing the same resonance but with an angle between the directions of the two dipoles. The scale bar represents 20 μm. (f) Experimentally retrieved real (black) and imaginary (gray) parts of the refractive index for the left circularly polarized wave. Negative index was attained at around 1.1 THz. (a), (b) From [8]. Reprinted with permission from AAAS. (c), (d) Reprinted by permission from Macmillan Publishers: Ltd: Nature, Copyright 2008 [11]. (e), (f) Reprinted figure with permission from [15], Copyright (2009) by the American Physical Society.

of the negative refractive index. We fabricated up to five layers of nanoring structures and performed the transmission measurement to retrieve the bulk negative index in the telecommunication wavelengths. In addition, we also carried out rigorous phase measurement on a 2-layer nanorings sample and extracted a polarization-independent negative index of −0.93 at 1900 nm wavelength.

Another way to attain negative index is through the use of chiral metamaterials. Chirality can be attained by engineering the cross coupling between the electric and magnetic dipoles along the same direction [13, 14]. This chirality will then act to lift the degeneracy of the two circularly polarized lights in such a way to decrease the refractive index of one circular polarization (till negative values) and increase the other. To demonstrate this, we devised a 3D gold microstructure (figure 1(e)) that produced a resonance with closely aligned effective electric and magnetic dipoles to generate strong chirality [15]. The subsequent fabrication and measurement indeed confirmed the attainment of negative index (with a minimum of −5) for the left-circularly polarized wave between 1.06 and 1.27 THz frequency range, as shown in figure 1(f). Interestingly, using such a deep subwavelength chiral building block, we also demonstrated photoinduced handedness switching with a much stronger electromagnetic effect than that of naturally available molecules [16].

One of the biggest motivations to build a NIM is to realize a perfect lens (as discussed in the next section). However, such a NIM has to be isotropic in all three directions. Using mixing theories, we showed that a plasmonic meta-atom with the right symmetry and gap opening can have overlapped electric and magnetic dipoles [17]. A random distribution of such meta-atoms, with adequate filling fraction, in a host medium will allow the realization of a 3D isotropic NIM. Another approach is to utilize both the plasmonic and Mie resonances in metallo-dielectric nanospheres [18]. Recently, we successfully synthesized random gold core and copper oxide shell nanoparticles with carefully designed electric and magnetic resonances to overlap at around 850 nm wavelength to attain the negative index property [19]. The spherical geometry of the core–shell nanoparticles ensures the NIM to be isotropic and polarization independent in all three different directions.

3. Superlenses to beat the diffraction limit

A conventional lens cannot focus light onto an area smaller than a square wavelength due to the loss of exponentially decaying evanescent waves which carry the subwavelength details of the imaged object. In 2000, Pendry showed that a slab of NIM could amplify the evanescent waves and restore all the deep subwavelength features, making it a perfect lens to surpass the diffraction limit [4]. However, the realization of such a perfect lens is extremely challenging as it requires an isotropic NIM with negligible loss.

Fortunately, one could relax the stringent requirement and still achieve subwavelength imaging by building a near-field superlens. In the near field, the electric and magnetic components are decoupled, so for the transverse magnetic (TM) polarization only negative permittivity is needed to construct a superlens. In our early experiment, we made a negative permittivity silver slab and experimentally verified the growth of evanescent waves in the near field (up to 30 times for an optimized thickness of 50 nm) [20]. To test the imaging capability of the superlens, we deposited 35 nm of silver on a well-planarized PMMA spacing layer sitting on top of a patterned chromium structures serving as the imaged objects [21]. By using a conventional i-line illumination (365 nm wavelength), we could directly record the reconstructed image on a photoresist spun on top of the silver superlens (figure 2(a)). Upon resist development, the subwavelength grating (with 60 nm half-pitch) and the 'NANO' objects were clearly resolved, as shown in figure 2(b), thereby proving the optical near-field superlensing effect down to $\lambda/6$.

Despite the ability to resolve well beyond the diffraction limit, the near field operation of the silver slab limited its potential applications. Our subsequent work therefore aimed to realize a far-field superlens, where by adding a subwavelength silver grating on the silver slab, we converted some of the enhanced evanescent waves into propagating waves [22]. Using this technique, we experimentally imaged a pair of 50 nm wide slits with a separation of 70 at 377 nm wavelength using a conventional optical microscope setup. It is important to note that the subdiffraction imaging capability can also be observed at other frequencies. For instance, we used the negative permittivity of perovskite oxides to realize a superlens in the mid-infrared regime [23]. Interestingly, in addition to using the superlens for imaging purposes, we also fabricated the metal slab on a flying head and realized a high-throughput maskless nanolithography beyond the diffraction limit [24, 25].

4. Hyperbolic metamaterials (HMMs)

To overcome the diffraction limit and form a magnified optical image in the far field, a cylindrically curved HMM, also known as a hyperlens, is proposed [26, 27]. HMMs are highly anisotropic engineered materials, named after their hyperbolic topology of iso-frequency contours. Hyperbolic dispersion originates from the opposite signs of permittivity or permeability tensor components for the in-plane (x, y) and out-of-plane (z) directions, such as $\varepsilon_{xx}\varepsilon_{zz} < 0$ and $\mu_{xx}\mu_{zz} < 0$. Unlike conventional isotropic materials ($\varepsilon_{xx} = \varepsilon_{yy} = \varepsilon_{zz}$) that has a spherical iso-frequency surface with bounded wave-vector components, the iso-frequency contour of a HMM takes the shape of an unbounded hyperbolic surface.

Therefore HMMs can support extremely large k-vectors, which are critical to resolve subwavelength features for super-resolution imaging [26, 27]. In our experimental demonstration, we fabricated a hyperlens by depositing 16 alternating layers of silver (35 nm) and alumina (35 nm) on a half-cylindrical cavity [28]. The metal and dielectric material, and the thickness were carefully chosen to yield an effective permittivity of $\varepsilon_r < 0$ and $\varepsilon_\theta > 0$ in the radial and azimuthal direction, respectively. The opposite signs of the permittivity thus enabled a nearly flat hyperbolic iso-frequency contour that not only allowed the retrieval of high wavevectors information, but also guided the radiation along the radial direction, as shown in figure 2(c). As the high-k evanescent waves traveled outward from the inner cylinder, the transverse wavevectors would adiabatically decrease till they became smaller than the light wavevectors and got converted to the propagating waves. Such a hyperlens configuration can therefore magnify the subwavelength details of the imaged object to above the diffraction limit and render them observable even in the far-field. At an ultraviolet wavelength of 365 nm, the hyperlens was able to resolve a pair of 35 nm wide lines with 150 nm spacing, and achieved a subdiffraction resolution of 130 nm with a magnification of about 2.3 (figure 2(d)). Later in 2010, we extended the one-dimensional subdiffraction resolving capability of the cylindrical hyperlens to two-dimensional by making a spherical hyperlens working at the visible wavelength of 410 nm [29].

Apart from imaging, HMMs can also exhibit unusual negative refraction because the direction of the group velocity ($\nabla_k\omega$) is always normal to the iso-frequency contour, which takes a hyperbolic shape in a HMM [30]. However, realizing a bulk HMM at optical frequencies is rather challenging due to the difficulty in fabrication and the material and resonant losses. By carefully designing a metallic wire array using effective medium theory, hyperbolic dispersion could be obtained even far away from the resonance, thus enabling operation over a broad frequency range while significantly reducing the resonant loss. In our experiment, we utilized electrochemical deposition process to fabricate high-quality silver nanowires array (60 nm diameter and 100 nm center-to-center distance) in a porous alumina host template and realized a broadband, low-loss bulk hyperbolic medium in the visible wavelengths [31]. Negative refraction was unambiguously measured for a wide range of incident angles with TM polarization at 660 and 780 nm wavelengths, as depicted in figures 3(a)–(c).

Owing to the unbounded hyperbolic iso-frequency contour, HMMs can ideally support diverging photonic density of states. According to the Fermi's golden rule, the spontaneous emission rate is proportional to the photonic density of states. Therefore, when an emitter is placed near the HMM, the spontaneous emission lifetime can be substantially reduced.

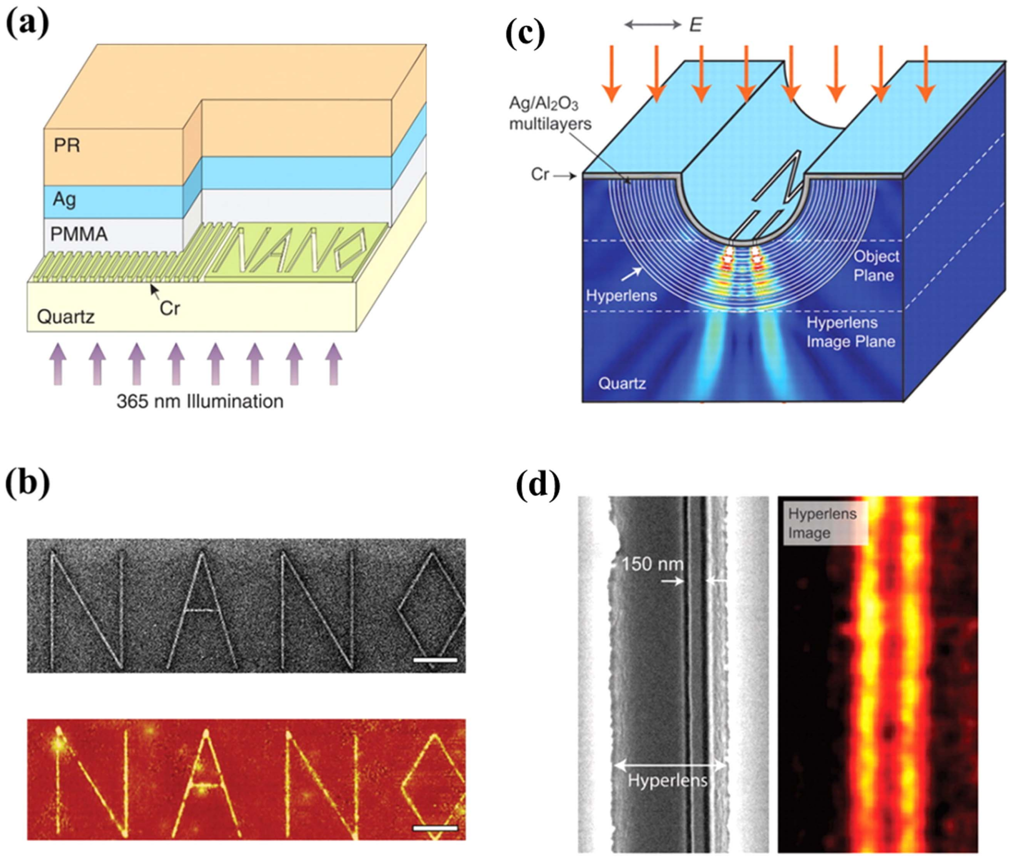

Figure 2. Superlens and hyperlens for super-resolution imaging. (a) A near-field superlens using the negative permittivity property of the silver slab to reconstruct subdiffraction image of the chromium (Cr) objects on the coated photoresist (PR) at 365 nm wavelength. (b) A focused ion beam image of an arbitrary 'NANO' object (top) that had a linewidth of 40 nm was used to test the performance of our near-field superlens. The atomic force microscope (AFM) scan of the developed image on the PR (bottom) showed that the object was clearly resolved beyond the diffraction limit. The scale bars represent 2 μm. (c) A cylindrical hyperlens consisted of silver (Ag) and alumina (Al_2O_3) multilayers magnified the high-k evanescent waves and converted them to propagating waves. (d) Using the hyperlens, a pair of 35 nm wide lines with 150 nm gap was clearly resolved with an illumination at 365 nm wavelength, beating the diffraction limit. (a), (b) From [21]. Reprinted with permission from AAAS. (c), (d) From [28] Reprinted with permission from AAAS.

To strongly confine the light to enhance the light–matter interaction, we realized an array of HMM nanopyramid cavity each consisting of three pairs of silver (20 nm) and germanium (30 nm) multilayers [32, 33], as shown in figures 3(d) and (e). We found that the HMM cavity followed an anomalous scaling law, where the higher-order resonances could occur at lower frequencies. Experimentally, we managed to achieve an optical cavity with physical size down to $\lambda/12$ (with ultrahigh effective indices up to 17.4) and a radiation quality factor as high as 4000, all due to the hyperbolic isofrequency contour (figure 3(f)). This gives rise to new possibilities in cavity quantum electrodynamics and nanoconfinement of light for sensing and communication applications.

In 2016, we demonstrated a magnetic HMM by fabricating a fishnet-like structure composed of 20-layer stack of gold and magnesium fluoride to attain opposite signs of the permeability tensor components, i.e. $\mu_{yy}\mu_{zz} < 0$ [34]. Unlike conventional electrical HMMs which are restricted to work only in the TM polarization, our magnetic HMM allows operation in the TE polarization and opens the door for free-space impedance matching. Our experiment also rigorously verified the topological phase transition between the elliptic and hyperbolic dispersion and showed strong enhancement of thermal emission using the magnetic HMM structure. Recently, we also proposed the use of cold atoms to build hyperbolic quantum metamaterials [35]. By controlling the coherent drive fields, we could attain anisotropic optical response and realize topologically reconfigurable atomic-lattice-based metamaterials with ultrafast time scales important for quantum sensing and quantum information processing.

5. Acoustic metamaterials

The concept of subwavelength structuring in metamaterials is general for all kinds of waves. Without limiting ourselves to high frequency THz and optical waves, we have utilized the metamaterial principle to engineer new acoustic material properties. We demonstrated an ultrasonic metamaterial with negative bulk modulus by making an array of Helmholtz resonators with subwavelength ($\lambda/5$) spacing in a fluid channel [36]. The Helmholtz resonator consisted of a rigid-walled cavity with a small opening, and was analogous to an inductor-capacitor (LC) circuit, as illustrated in figure 4(a).

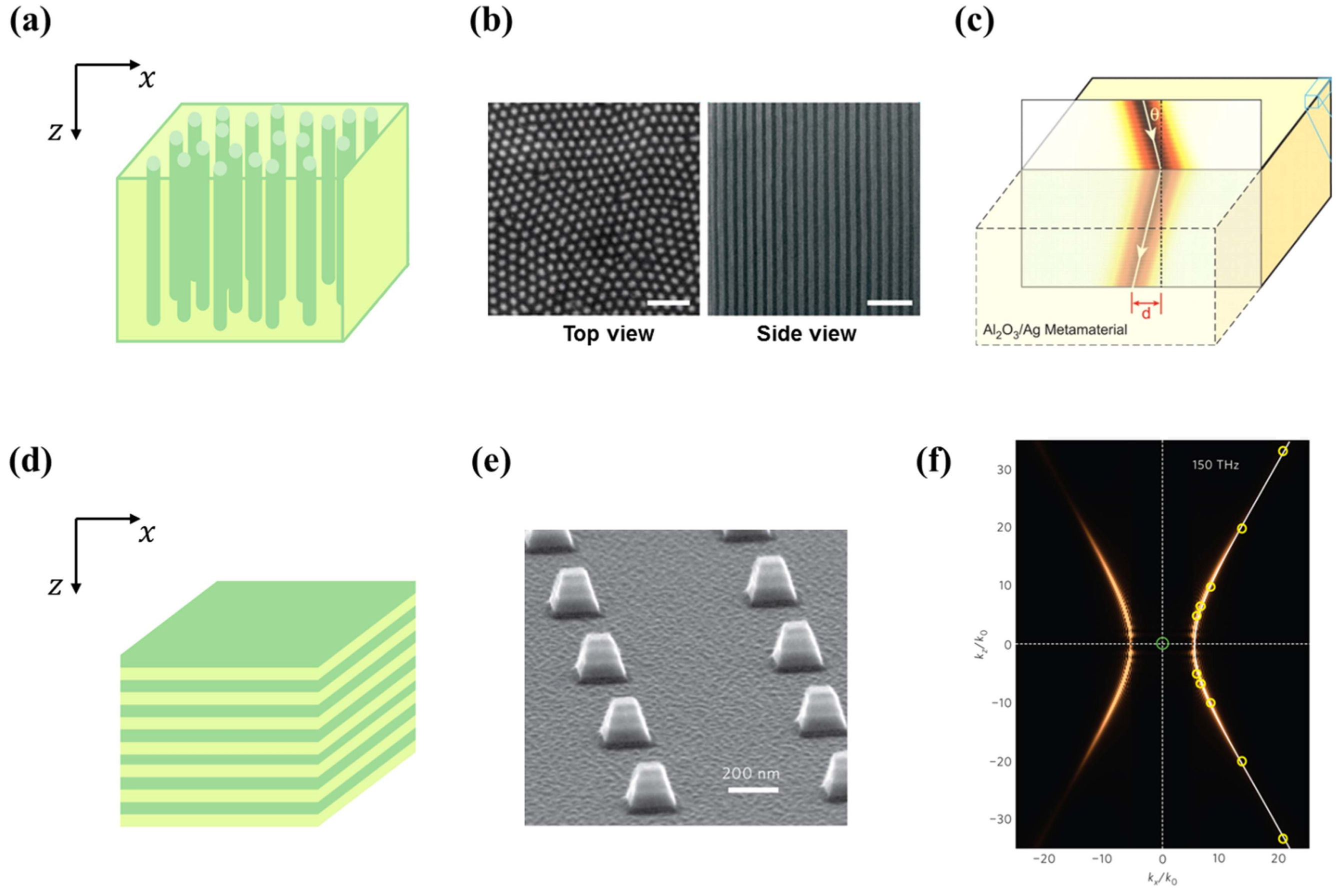

Figure 3. Hyperbolic metamaterials for negative refraction and anomalous optical cavities. (a) Illustration and (b) SEM images of silver nanowires array in a porous alumina host template which forms a bulk hyperbolic medium and negatively refracts the incident light. The scale bars represent 500 nm. (c) The light exiting the bulk hyperbolic metamaterial surface showed negative refraction of TM-polarized light. (d) Schematic and (e) SEM images of an array of nanopyramid hyperbolic cavity composed of silver and germanium multilayers. (f) The hyperbolic iso-frequency contour displayed by the nanopyramid hyperbolic cavity enabled extreme light confinement within a subwavelength cavity volume. (b), (c) From [31]. Reprinted with permission from AAAS. (e), (f) Reprinted by permission from Macmillan Publishers Ltd: Nature Photonics [33], Copyright 2012.

By designing the volume of the cavity and the size of the opening, we achieved a strong resonance around 32 kHz and experimentally measured a negative group velocity of the propagating ultrasonic waves (figure 4(b)). Such a negative modulus ultrasonic metamaterial can introduce resonant surface modes [37] that enhance the evanescent spectrum from the subwavelength objects and paves the way for acoustic superlens in super-resolution imaging.

Another approach to restore the evanescent waves is by strongly coupling them with the Fabry–Perot resonance mode which displayed a rather flat dispersion curve for a wide range of wavevectors, while maintaining unity modulus of the zero-order transmission coefficient. By making a 3D acoustic metamaterial with deep-subwavelength periodic square hole arrays (figure 4(c)), we successfully resolved an object feature size of $\lambda/50$ at an operating frequency of 2.18 kHz (figure 4(d)) [38]. The physics behind it is rather similar to the canalization phenomenon previously used to reconstruct subwavelength information from the input to the output surface of a system. To realize a broadband subdiffraction acoustic imaging, we also devised an acoustic hyperlens which utilized the non-resonant hyperbolic dispersion to convert the high-k evanescent waves to propagating waves [39]. The structure was made of 36 brass fins (running in the radial direction) in a half-cylinder configuration with an aluminum cover to confine the sound propagation region to two-dimensions, as shown in figure 4(e). Our pressure measurement results showed that the acoustic hyperlens could resolve and magnify two subdiffraction sound sources over a broad frequency range from 4.2 to 7 kHz (figure 4(f)). We believe there are plenty of opportunities in the field of acoustic metamaterials, as the challenging subwavelength structuring in optics is no longer a limiting factor in acoustics due to its much larger unit cell size. For instance, we recently realized an acoustic zero refractive index material [40] and an acoustic cloaking device [41]. In addition, acoustic metamaterials can be dynamically controlled at a speed much faster than their operating frequency and thus enable many novel active acoustic devices with unprecedented properties.

6. Transformation optics: optical cloaking and Janus optics

For a material with a known refractive index distribution, the light trajectory can be estimated using the Fermat's principle. Inversely, one can design arbitrary light path by spatial

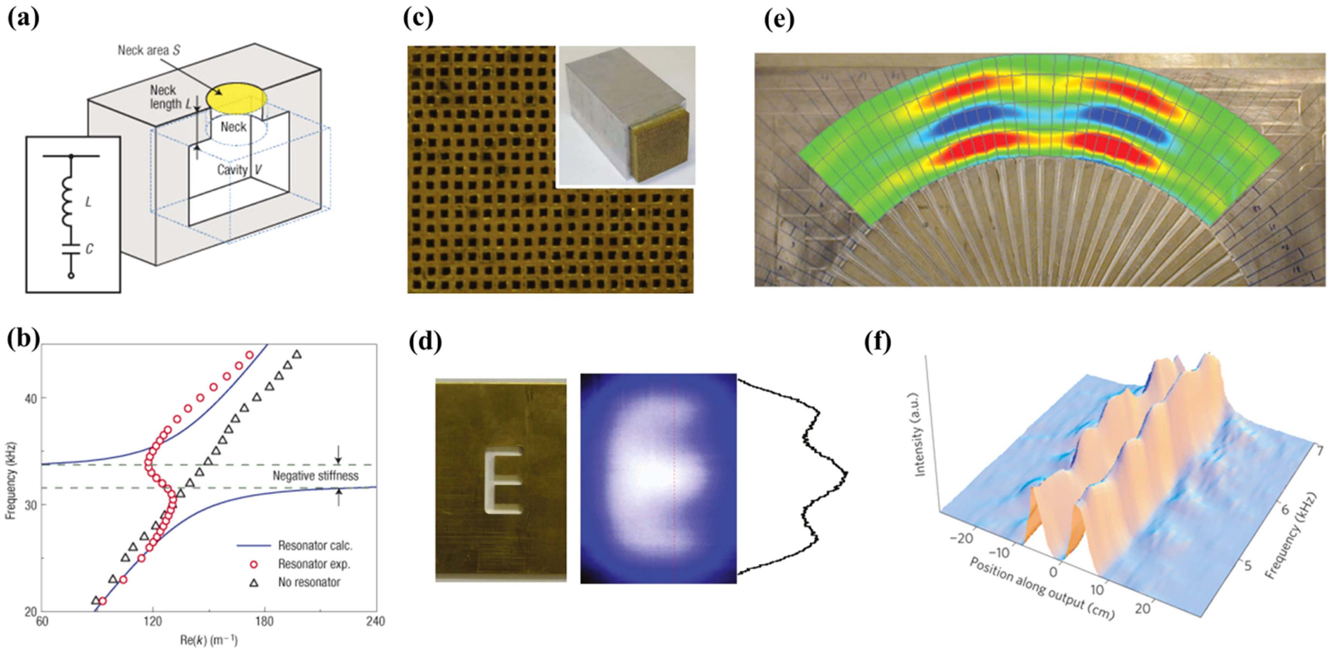

Figure 4. Acoustic negative stiffness metamaterials, superlens and hyperlens. (a) A Helmholtz resonator can be made by carving out a cavity within a rigid material and connecting it to the outside via a neck, equivalent to an inductor (L)—capacitor (C) circuit in electronics. (b) A 1D array of carefully designed Helmholtz resonators with subwavelength spacing resulted in negative stiffness property, as measured experimentally at around 32 kHz. (c) An acoustic holey-structured metamaterial consisted of 40×40 square brass alloy tubes was built to demonstrate deep subwavelength imaging. (d) Using the holey-structured metamaterial, a letter 'E' with 3.18 mm linewidth was resolved at wavelength over 50 times larger. (e) 36 brass fins extending in the radial direction was carefully designed in a half-cylinder configuration to realize the acoustic hyperlens. A dual-source subdiffraction-limited object was placed close to the inner circle of the hyperlens. The colors showed the measured pressure distribution which clearly separated and magnified the acoustic waves exiting the hyperlens, (f) the pressure intensity measured at the outer edge of the hyperlens demonstrated its broadband subdiffraction acoustic imaging capability from 4.2 to 7 kHz, which corresponded to about $\lambda/7$ to $\lambda/4$ resolutions. (a), (b) Reprinted by permission from Macmillan Publishers Ltd: Nature Materials [36], Copyright 2006. (c), (d) Reprinted by permission from Macmillan Publishers Ltd: Nature Physics [38], Copyright 2010. (e), (f) Reprinted by permission from Macmillan Publishers Ltd: Nature Materials [39], Copyright 2009.

engineering of the refractive index satisfying certain coordinate transformation conditions. This is because Maxwell's equations retain the same form under coordination transformations. The new permittivity ε' and permeability μ' are related to the original ε and μ via a Jacobian matrix that describes the geometrical variation between the original (x) and the transformed space (x') [5]. A careful design and arrangement of the exotic metamaterial elements in the transformed space will therefore enable ultimate control of light and realize many novel optical effects. In 2006, Pendry, Schurig and Smith showed that such a transformation optics principle can be used to build an invisibility cloak [5]. Soon after, the invisibility cloak was experimentally realized in the microwave frequencies with spatially varying copper plates to meet the ε and μ requirements [42]. However, it is difficult to implement such a cloak in the optical frequencies due to the stringent requirement of anisotropic material properties with extreme ε and μ values. It was later proposed that another coordinate transformation technique based on conformal mapping could enable the use of isotropic materials with moderate refractive index distribution. As the cloak mainly works in the reflection mode, it is called as a carpet cloak [43]. In 2009, we experimentally realized such a cloak in the near-infrared wavelengths [44]. Focused ion beam patterning was performed on a silicon-on-insulator wafer to obtain varying subwavelength hole sizes, as shown in figure 5(a). Based on the effective medium approximation, a spatial distribution of refractive index can therefore be realized. Despite the presence of a bump object, the reflected light showed a single spot of Gaussian beam similar to reflection off a flat surface, and the scattering from the object geometry was no longer visible (figure 5(b)). Since there was no resonance process involved, the cloaking effect was observed for a broad wavelength range from 1400 to 1800 nm. In a follow-up experiment, we realized a carpet cloak in the visible wavelengths using a silicon nitride on nanoporous oxide material platform [45].

In addition to cloaking, transformation optics can help to realize many other interesting optical effects, such as focusing, beam shifting and bending. Instead of limiting the device to perform a single task, we believe transformation optics could enable multifunctional optical devices. By compressing the device boundaries into an inhomogenous physical space of varying hole densities (figure 5(c)), we experimentally demonstrated a Janus optical device which behaved like a lens in one direction, and like a beam shifter in the other direction [46], as shown in figure 5(d). This not only allows high-density integration of optical elements, but also presents a new path to scale down the size of photonic integrated circuits.

Even though transformation optics was originally proposed to manipulate propagating waves, the same principle can be

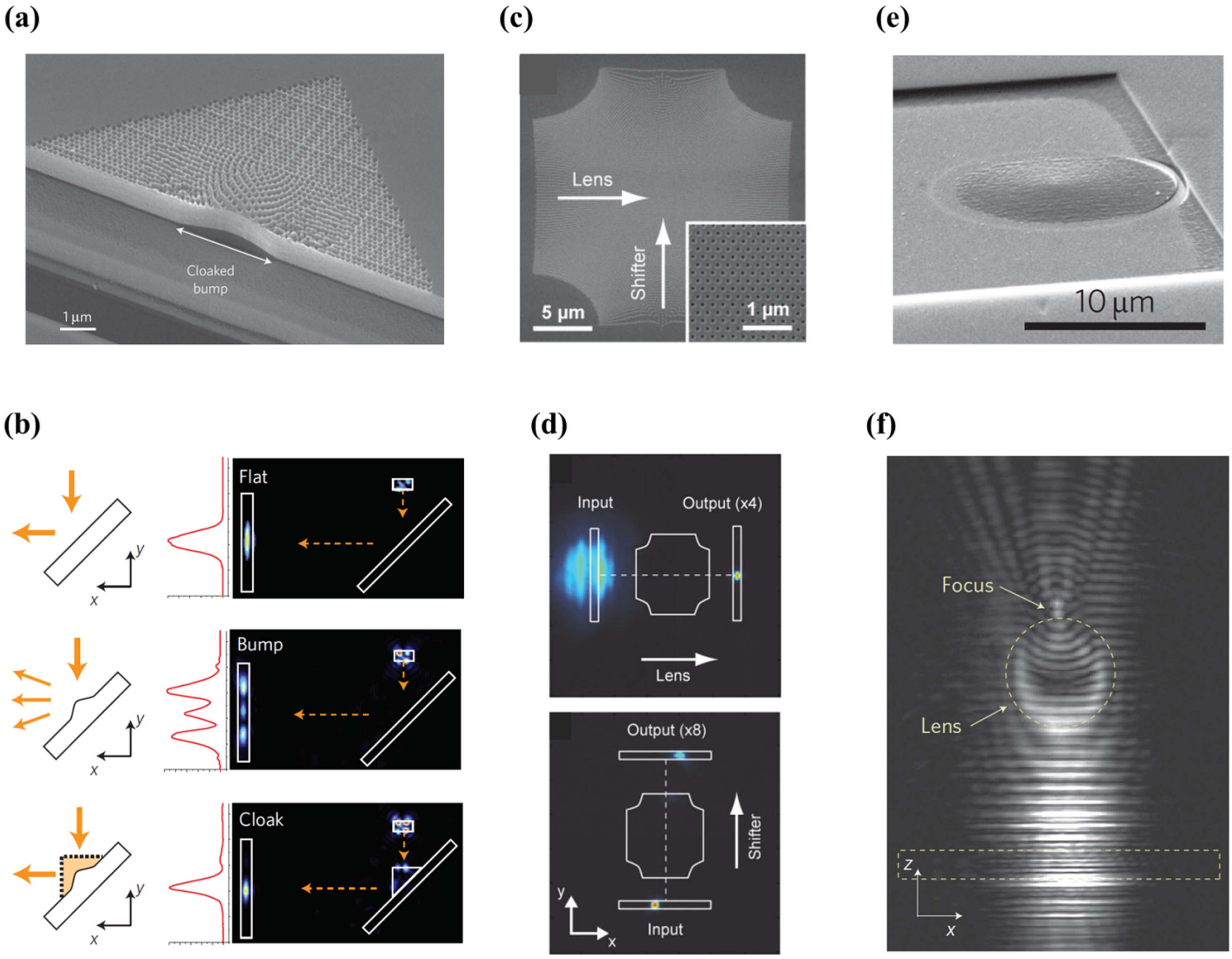

Figure 5. Transformation optics enables an invisibility cloak, a multifunctional Janus device and a plasmonic Luneburg lens. (a) SEM image of a carpet cloak fabricated on a silicon-on-insulator (SOI) substrate, where the spatially varying effective index is attained through the patterning of different hole sizes. (b) When the surface is flat, a single Gaussian beam spot is detected; whereas for a surface with a bump, three distinct beam spots are measured due to the scattering from the bump. However, with the fabricated cloak, the single Gaussian beam spot is perfectly restored as if the bump does not exist there. (c) SEM image of a fabricated multifunctional Janus device, with increasing hole density from the device boundary towards the center. (d) Measurement results showed that the device functioned as a lens in the horizontal direction, and as a beam shifter in the vertical direction. (e) SEM image of a fabricated Luneburg lens, where the mode index is spatially varied using gray-scale lithography to gradually change the PMMA thickness. (f) The focusing of the surface plasmon polariton is experimentally observed using a leakage radiation microscopy. (a), (b) Reprinted by permission from Macmillan Publishers Ltd: Nature Materials [44], Copyright 2009. (c), (d) [46] John Wiley & Sons. Copyright © 2010 WILEY-VCH Verlag GmbH & Co. KGaA, Weinheim. (e), (f) Reproduced from [48]. CC BY 3.0.

applied to the near-field evanescent waves as well, such as the surface plasmon polariton (SPP) at the metal-dielectric interface. By engineering the index distribution of the dielectric layer, we showed that one can bend the SPP, or even reroute the SPP to avoid any surface protrusion that can scatter the wave [47]. Transformation optics with SPP opens the door for new plasmonic devices with unique functionality. Experimentally, as shown in figure 5(f), we realized a plasmonic Luneburg lens which can focus the SPP to a single spot at the edge of the lens [48]. This was achieved by using gray-scale lithography to gradually vary the thickness of a PMMA layer to satisfy the index profile of a Luneburg lens (figure 5(e)). Remarkably, such a simple Luneburg lens can operate over a broad wavelength range with minimal scattering loss.

7. Nonlinear metamaterials: lifting the phase matching requirement and testing of Miller's rule

Despite the many extraordinary properties promised, linear metamaterials are ultimately constrained by the properties of linear time invariant systems. For example, they cannot amplify or change the frequency of a photon. Nonlinearity, from added nonlinear materials or the intrinsic nonlinearity of metamaterial constituents such as noble metals, allows metamaterials to move beyond the constraints of linear systems. In 2012, our group experimentally demonstrated nonlinear negative refraction by four-wave mixing in a thin nanostructure gold film (figures 6(a) and (b)) [49]. It is challenging to attain negative refraction using linear optics

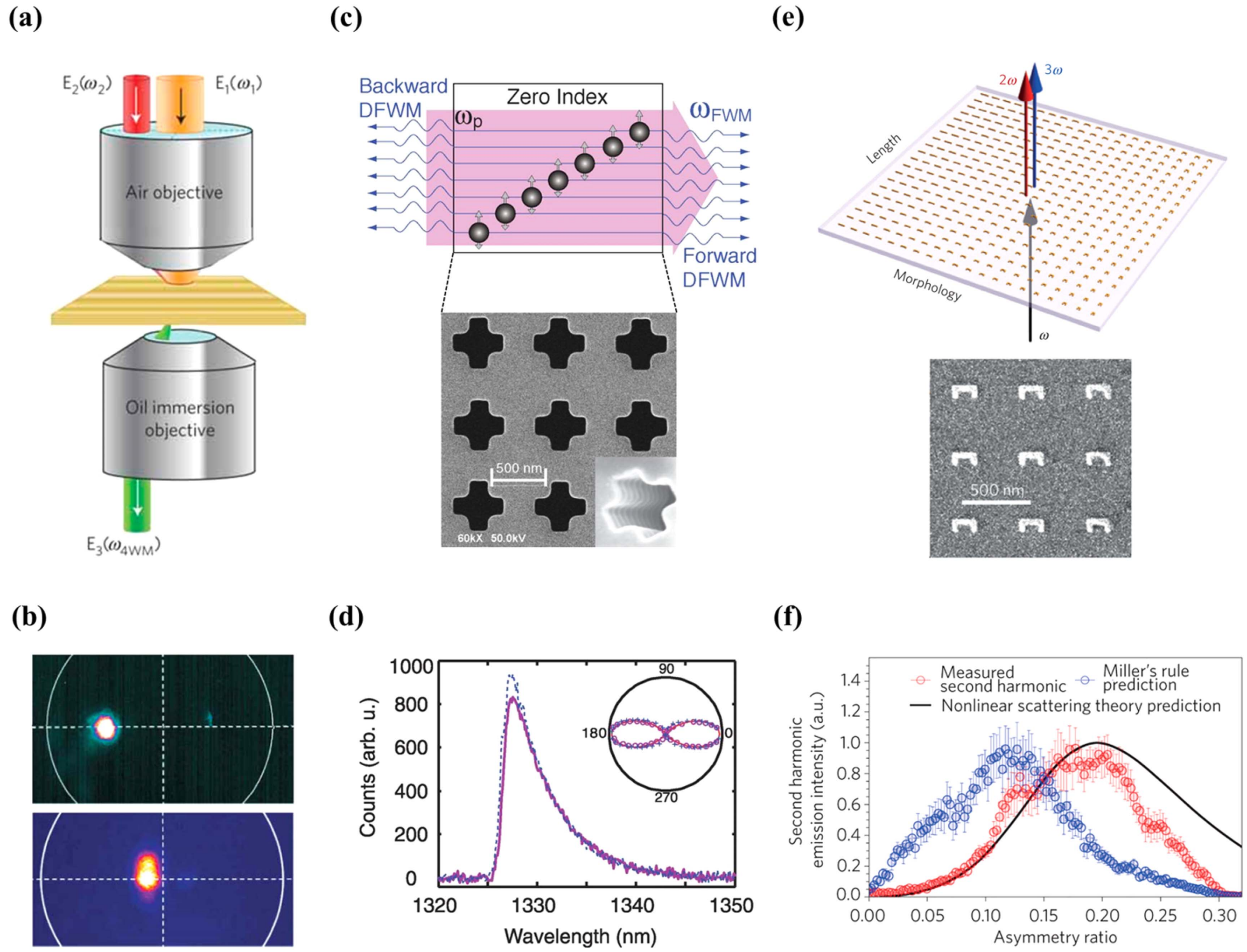

Figure 6. Nonlinear metamaterials for negative refraction, bi-directional phase-matching and nonlinear emission. (a) Four-wave mixing (FWM) in a thin nanostructured gold film can produce an idler which mimics negative refraction with enhanced efficiency due to localized plasmon resonance. (b) The measured Fourier plane image of the probe beam (top) and the forward FWM signal (bottom) both showed light spots located at the same side, thus proving the negative refraction behavior. (c) In a zero index (multilayer fishnet) material, the phase is uniform across the entire material and FWM can be generated in both the forward and backward directions. (d) Experimental demonstration of nearly identical forward (purple) and backward (blue) FWM in a zero index metamaterial. Inset shows the $\cos^6\theta$ dependence of FWM emission on pump polarization (with a horizontally polarized analyzer) typical for a $\chi^{(3)}$ response. (e) Experimental test of nonlinear scattering theory by measuring second harmonic generation as a function of nanostructure size and morphology. (f) Nonlinear scattering theory was found to accurately predict the relative nonlinear emission of different nanostructures, but not the well-known Miller's rule. (a), (b) Reprinted by permission from Macmillan Publishers Ltd: Nature Materials [49], Copyright 2012. (c), (d) From [51]. Reprinted with permission from AAAS. (e), (f) Reprinted by permission from Macmillan Publishers Ltd: Nature Materials [52], Copyright 2015.

because it requires both negative permittivity and negative permeability, or a hyperbolic medium. However, nonlinear optics can actually achieve negative refraction using four-wave mixing process and it has the potential to produce a perfect lens [50].

Phase mismatch, which occurs when the photons involved in a nonlinear process do not fulfill momentum conservation, is a major impediment to efficient frequency conversion in nonlinear optics. A number of successful phase matching schemes have been developed in the past, such as the angle phase matching, birefringent phase matching and quasi-phase matching, but none enables simultaneous phase matching of forward and backward degenerate four-wave mixing. Zero index metamaterials (ZIMs) [11] solve this problem by creating a uniform phase throughout the medium. ZIMs essentially relieve the phase matching requirements and enable simultaneous phase matching of forward and backward four-wave mixing as shown in figure 6(c). To demonstrate this effect, we designed and fabricated a relatively high transmission zero index fishnet metamaterial consisting of 20 alternating gold (30 nm) and magnesium fluoride (50 nm) layers on a suspended silicon nitride membrane [51]. We pumped the fishnet metamaterial with ultrashort laser pulses and measured the degenerate four-wave mixing (DFWM) in the forward and backward directions. We observed equal four-wave mixing in both forward and backward directions near the zero index frequency (figure 6(d)). As for the negative index wavelength, we showed that four-wave mixing was predominantly in the forward direction similar to the case of conventional positive index materials.

The well-known Miller's rule established an empirical, yet powerful relationship between linear and nonlinear responses of the natural crystals. The rule has been very effective in predicting nonlinear properties through the measurement of its linear optical responses. But does Miller's rule still apply in metamaterials? We found that in general Miller's rule does not apply in metamaterials mainly due to the mismatch between the linear and nonlinear modes generated in metamaterials [52], while in atomic crystals this is not an issue. The next question is how can we then predict nonlinear properties from linear properties in metamaterials? For this purpose, we developed a theoretical treatment of the nonlinear scattering theory in metamaterials, which gave a rigorous solution of Maxwell's equations for arbitrary nonlinear susceptibility tensors and arbitrary geometries [52]. This technique can be implemented in commercial finite element solvers. We experimentally tested nonlinear scattering theory in metamaterials by fabricating arrays of nanostructures in which the length and morphology varied along the horizontal and vertical axes, as shown in figure 6(e). We measured the second harmonic emission with scanning confocal nonlinear microscopy. We found that nonlinear scattering theory provided an accurate description of the nonlinear scattering cross section; whereas a nonlinear oscillator model based on the linear susceptibilities failed to accurately predict the relative nonlinearities (figure 6(f)). Nonlinearity expands the capabilities of metamaterials and has the potential to advance nonlinear optical physics and enable new nonlinear optical devices.

8. Quantum metamaterials: photonic spin Hall effect (PSHE), anti-Hermitian coupling and scalable quantum engineering

Similar to the transformation optics scheme of spatially engineering the refractive indices, manipulation of the phase at each point on a surface can lead to new device functionalities. A metasurface typically consists of an optically thin layer of spatially varying subwavelength structures to locally tailor the phase of an electromagnetic field and control its propagation. In the past, metasurfaces have enabled a variety of unique phenomena, such as broadband negative refraction, unidirectional surface wave coupling, flat lenses and waveplates, and ultra-thin holograms [53]. However, all the metasurfaces demonstrated to date relied on the patterning of distributed nanostructures on a flat surface to introduce the additional phase. Instead, we took an opposite approach whereby patterning nanoantennas on a curved surface, we could compensate the extra phase at each point caused by the height difference and realign the wavefront [54]. We envision such a simple image manipulation technique will find many interesting applications in the display technologies.

More interestingly, metasurfaces can be an important tool to control the spin polarization of light. When light is refracted at different angles, spin-polarization dependent geometric phase will emerge and result in a split of the light beam in the transverse direction at the interface, a PSHE. However, this effect is usually very small and the amount of splitting can only be detected by performing quantum weak measurements with pre- and post-selection of spin states [55]. To enhance the transverse splitting in polarizations, one can introduce inversion symmetry breaking metasurfaces. In our experiment, we used a spatially varying V-shaped nanoantenna metasurface to generate a linear phase gradient that bends light at a refraction angle much greater than the one achievable with a common dielectric interface [56]. As shown in figure 7(a), the PSHE manifested by the metasurface can be directly measured with a camera by recording the polarization dependent transport with the Stokes parameters. Incident light with opposite helicity are both anomalously refracted at the same angle but transversely transported against each other (figure 7(b)). Therefore, the use of metasurface will open a new degree of freedom to control the flow of light and enable spin polarization dependent novel functionalities.

While the direct near-field coupling between the neighboring meta-atoms is typically not desired in the metasurface design, it can be carefully engineered to attain novel optical properties. In 2012, we demonstrated a purely imaginary anti-Hermitian coupling by designing the near-field coupling to cancel out the Cauchy principle value of the indirect coupling (mediated by radiative channels) [57]. In such a system, even though an impinging light wave can simultaneously excite all the meta-atoms, constructive interference only occurs at a single meta-atom while the rest of the meta-atoms will experience destructive interference. This enables a spatially localized state with a much narrower spectrum compare to the same metasurface without any near-field coupling. In our experiment, we fabricated a metasurface consisting of 5 pairs of plasmonic nanoantenna with carefully designed near-field coupling (figure 7(c)), and showed that each of the antenna can be individually excited despite them being closely packed within only $\lambda/15$ separation (figure 7(d)). We believe the imaginary coupling in metamaterial design can be crucial for light manipulation at deep subwavelength scale, besides enabling spectrum splitting and wavelength multiplexing for integrated optics.

The phase engineering capability of a metasurface is not limited to classical systems. In 2015, we showed that metasurface could control the radiative decay of quantum emitters even at macroscopic distance apart (figure 7(e)), demonstrating a path towards quantum metamaterials [58]. With the right design of the metasurface's phase profile and polarization response, the incident field can be selectively reflected and refocused at the source position for one polarization, but defocused for another polarization (figure 7(f)). This helps to create anisotropic quantum vacuum and facilitate quantum interference between the radiative decay channels of the atomic emitter with orthogonal transitions, which is forbidden in free-space. The use of metasurface to remotely engineer the quantum vacuum and couple quantum states opens the door

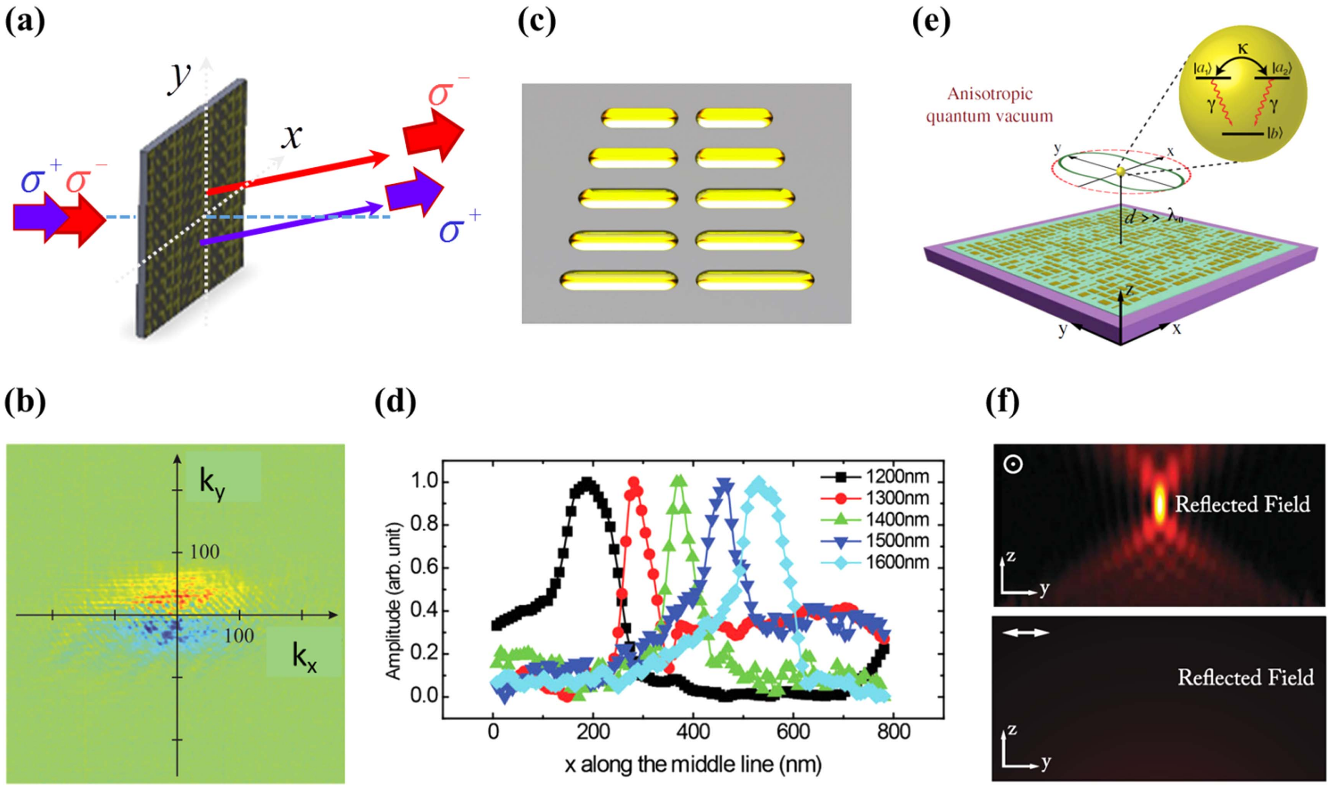

Figure 7. Optical metasurface for photonic spin Hall effect (PSHE), anti-Hermitian coupling and remote quantum interference. (a) Illustration of the PSHE. Lights with opposite helicity were anomalously refracted at the same refraction angle determined by the linear phase gradient of the inversion symmetry-breaking metasurface. However, the lights would experience a helicity dependent split in the transverse direction. (b) For an *x*-polarized beam along the phase gradient direction, a transverse split manifesting a giant PSHE was measured experimentally using the polarization-resolved detection, where the red and blue color represented the right and left circular polarizations, respectively. (c) Schematic of a plasmonic antenna array with varying lengths and close spacing to introduce the near-field interaction which can result in anti-hermitian imaginary coupling. (d) The near-field measurement results at different wavelengths showing how each antenna can be individually excited from the far field. (e) Metasurface enables anisotropic decay of a linear dipole at macroscopic distance. For a quantum emitter, such anisotropic quantum vacuum induces quantum interference between the radiative decay channels. (f) The phase and polarization response of the subwavelength nanoantennas are engineered to strongly reflect the incident field back to its source for the *x* dipole (top), but defocus the incident field for the y dipole (bottom), which gives rise to an anisotropic quantum vacuum. (a), (b) From [56]. Reprinted with permission from AAAS. (c), (d) Reprinted figure with permission from [57], Copyright 2012 by the American Physical Society. (e), (f) Reprinted figure with permission from [58], Copyright 2015 by the American Physical Society.

for long-range light-atom interactions that is the key for scalable quantum information processing.

In 2014, we showed that the metamaterial concept can significantly improve the detection of quantum signals in extremely sensitive experiments, approaching even the quantum-noise-limited performance [59]. We developed a nonlinear resonant phase matching technique whereby introducing an array of deep subwavelength resonators in the transmission line, large amplifier gain exceeding 20 dB over a broad 3 GHz bandwidth was experimentally achieved, with the capability to read out 20 superconducting qubits simultaneously [60]. Such a metamaterial-based quantum Josephson amplifier will find useful applications in microwave metrology, quantum electronics and solid-state quantum information processing. In fact, metamaterials can also be utilized to test the very fundamental quantum mechanics principle. In our recent experiment, we sent single photons through a Sagnac interferometer setup which contained a NIM (negative phase) and a nematic liquid crystal (positive phase) to test the phase commutativity and hence placed a bound on the hyper-complex quantum theory [61]. Therefore, we envision the integration between metamaterials and the field of quantum optics will open many exciting possibilities.

9. Conclusion and future directions

Over the last 15 years, metamaterials research has grown tremendously from theoretical curiosity to ground-breaking experiments demonstrating rich physics and enormous potentials for technological advancements. In addition to extending the metamaterial concept from microwave to acoustics, terahertz and optical regimes, we have shown that the engineering of subwavelength structures enabled super-resolution imaging, spontaneous emission rate enhancement, invisibility cloaking, efficient nonlinear generation, spin manipulation and many other exciting phenomena. Looking into the future, we believe many of the metamaterial concepts can be applied to the quantum systems to solve complex problems and trigger new possibilities. In 2008, we carried over the invariant coordinate transformation of the Maxwell's equations (used in transformation optics) to the time independent Schrodinger equation for quantum waves [62]. Our calculation showed that a concentric optical lattice with the right design of the potential and effective mass can enable cloaking of cold atoms. Interestingly, quantum phenomena also inspired the development of metamaterials research. We showed that an optical response resembling the electromagnetically induced transparency in atomic system can be attained by coupling a radiative plasmonic antenna with a subradiant (dark) antenna in the near field [63]. This plasmon induced transparency leads to a narrow transmission peak within a broad absorption spectrum and can be extremely useful for slow light applications. In addition, due to the similarity between the time dependent Schrodinger equation and the paraxial diffraction equation, one can realize the quantum mechanical parity-time (PT) symmetry in optical systems [64]. PT symmetry is interesting because it can lead to both the real and imaginary eigenvalue solutions and a crossover exceptional point. While traditional metamaterials focus on realizing unusual real part of the refractive index, engineering of the imaginary part of index (i.e. the gain and loss) satisfying PT symmetry can lead to many novel phenomena. For example, we realized a single mode microring laser by taking advantage of the unique complex conjugate imaginary eigenvalue solutions supported by the PT broken phase [65]. More recently, we also utilized PT symmetry to realize a single device for both lasing and anti-lasing [66]. We therefore believe that engineering metamaterials in the complex space could be the new key to search for extraordinary device performance for the many years to come.

Acknowledgements

This work was primarily funded by the "Light–Material Interactions in Energy Conversion" Energy Frontier Research CEnter, funded by the US Department of Energy, Office of Science, Office of Basic Energy Sciences under Award Number DE-AC02-05CH11231. X Z acknowledges support from Samsung Electronics. Y W acknowledges support from the Office of Naval Research (ONR) MURI program under Grant No. N00014-13-1-0678.

References

[1] Veselago V G 1968 The electrodynamics of substances with simultaneously negative values of ε and μ *Sov. Phys.—Usp.* **10** 509–14
[2] Pendry J B, Holden A J, Stewart W J and Youngs I 1996 Extremely low frequency plasmons in metallic mesostructures *Phys. Rev. Lett.* **76** 4773–6
[3] Pendry J B, Holden A J, Robbins D J and Stewart W J 1999 Magnetism from conductors and enhanced nonlinear phenomena 1999 *IEEE Trans. Microw. Theory Tech.* **47** 2075–84
[4] Pendry J B 2000 Negative refraction makes a perfect lens *Phys. Rev. Lett.* **85** 3966–9
[5] Pendry J B, Schurig D and Smith D R 2006 Controlling electromagnetic fields *Science* **312** 1780–2
[6] Shelby R A, Smith D R and Schultz S 2001 Experimental verification of a negative index of refraction *Science* **292** 77–9
[7] http://xlab.me.berkeley.edu/MURI/muri.html
[8] Yen T-J, Padilla W J, Fang N, Vier D C, Smith D R, Pendry J B, Basov D N and Zhang X 2004 Terahertz magnetic response from artificial materials *Science* **303** 1494–6
[9] Shalaev V M, Cai W S, Chettiar U K, Yuan H K, Sarychev A K, Drachev V P and Kildishev A V 2005 Negative index of refraction in optical metamaterials *Opt. Lett.* **30** 3356–8
[10] Zhang S, Fan W, Panoiu N C, Malloy K J, Osgood R M and Brueck S R J 2005 Experimental demonstration of near-infrared negative-index metamaterials *Phys. Rev. Lett.* **95** 137404
[11] Valentine J, Zhang S, Zentgraf T, Ulin-Avila E, Genov D A, Bartal G and Zhang X 2008 Three-dimensional optical metamaterial with a negative refractive index *Nature* **455** 376–9
[12] Kante B, Park Y-S, O'Brien K, Shuldman D, Lanzillotti-Kimura N D, Wong Z J, Yin X and Zhang X 2012 Symmetry breaking and optical negative index of closed nanorings *Nat. Commun.* **3** 1180
[13] Tretyakov S, Nefedov I, Sihvola A, Maslovski S and Simovski C 2003 Waves and energy in chiral nihility *J. Electromagn. Waves Appl.* **17** 695–706
[14] Pendry J B 2004 A chiral route to negative refraction *Science* **306** 1353–5
[15] Zhang S, Park Y-S, Li J, Lu X, Zhang W and Zhang X 2009 Negative refractive index in chiral metamaterials *Phys. Rev. Lett.* **102** 023901
[16] Zhang S *et al* 2012 Photoinduced handedness switching in terahertz chiral metamolecules *Nat. Commun.* **3** 942
[17] Kante B, O'Brien K, Niv A, Yin X and Zhang X 2012 Proposed isotropic negative index in three-dimensional optical metamaterials *Phys. Rev.* B **85** 041103
[18] Paniagua-Dominguez R, Lopez-Tejeira F, Marques R and Sanchez-Gil J A 2011 Metallo-dielectric core–shell nanospheres as building blocks for optical three-dimensional isotropic negative-index metamaterials *New J. Phys.* **13** 123017
[19] Yang S, Ni X, Kante B, Zhu J, O'Brien K, Wang Y and Zhang X 2016 *Experimental demonstration of optical metamaterials with isotropic negative index* (CLEO:2016 FTh3D.3) (https://doi.org/10.1364/CLEO_QELS.2016.FTh3D.3)
[20] Liu Z, Fang N, Yen T-J and Zhang X 2003 Rapid growth of evanescent wave by a silver superlens *Appl. Phys. Lett.* **83** 5184–6
[21] Fang N, Lee H, Sun C and Zhang X 2005 Sub-diffraction-limited optical imaging with a silver superlens *Science* **308** 534–7
[22] Liu Z, Durant S, Lee H, Pikus Y, Fang N, Xiong Y, Sun C and Zhang X 2007 Far-field optical superlens *Nano Lett.* **7** 403–8
[23] Kehr S C *et al* 2010 Near-field examination of perovskite-based superlenses and superlens-enhanced probe-object coupling *Nat. Commun.* **2** 249
[24] Srituravanich W, Pan L, Wang Y, Sun C, Bogy D B and Zhang X 2008 Flying plasmonic lens in the near field for high-speed nanolithography *Nat. Nanotechnol.* **3** 733–7
[25] Pan L *et al* 2011 Maskless plasmonic lithography at 22 nm resolution *Sci. Rep.* **1** 175
[26] Jacob Z, Alekseyev L V and Narimanov E 2006 Optical hyperlens: far-field imaging beyond the diffraction limit *Opt. Express* **14** 8247–56

[27] Salandrino A and Engheta N 2006 Far-field subdiffraction optical microscopy using metamaterial crystals: theory and simulations *Phys. Rev.* B **74** 075103
[28] Liu Z, Lee H, Xiong Y, Sun C and Zhang X 2007 Far-field optical hyperlens magnifying sub-diffraction-limited objects *Science* **315** 1686
[29] Rho J, Ye Z, Xiong Y, Yin X, Liu Z, Choi H, Bartal G and Zhang X 2010 Spherical hyperlens for two-dimensional sub-diffractional imaging at visible frequencies *Nat. Commun.* **1** 143
[30] Smith D R and Schurig D 2003 Electromagnetic wave propagation in media with indefinite permittivity and permeability tensors *Phys. Rev. Lett.* **90** 077405
[31] Yao J, Liu Z, Liu Y, Wang Y, Sun C, Bartal G, Stacy A M and Zhang X 2008 Optical negative refraction in bulk metamaterials of nanowires *Science* **321** 930
[32] Yao J, Yang X, Yin X, Bartal G and Zhang X 2011 Three-dimensional nanometer-scale optical cavities of indefinite medium *Proc. Natl Acad. Sci. USA* **108** 11327–31
[33] Yang X, Yao J, Rho J, Yin X and Zhang X 2012 Experimental realization of three-dimensional indefinite cavities at the nanoscale with anomalous scaling laws *Nat. Photon.* **6** 450–4
[34] Kruk S S, Wong Z J, Pshenay-Severin E, O'Brien K, Neshev D N, Kivshar Y S and Zhang X 2016 Magnetic hyperbolic optical metamaterials *Nat. Commun.* **7** 11329
[35] Jha P K, Mrejen M, Kim J, Wu C, Wang Y, Rostovtsev Y V and Zhang X 2016 Coherence-driven topological transition in quantum metamaterials *Phys. Rev. Lett.* **116** 165502
[36] Fang N, Xi D, Xu J, Ambati M, Srituravanich W, Sun C and Zhang X 2006 Ultrasonic metamaterials with negative modulus *Nat. Mater.* **5** 452–6
[37] Ambati M, Fang N, Sun C and Zhang X 2007 Surface resonant states and superlensing in acoustic metamaterials *Phys. Rev.* B **75** 195447
[38] Zhu J, Christensen J, Jung J, Martin-Moreno L, Yin X, Zhang X and Garcia-Vidal F J 2010 A holey-structured metamaterial for acoustic deep-subwavelength imaging *Nat. Phys.* **7** 52–5
[39] Li J, Fok L, Yin X, Bartal G and Zhang X 2009 Experimental demonstration of an acoustic magnifying hyperlens *Nat. Mater.* **8** 931–4
[40] Dubois M, Shi C, Zhu X, Wang Y and Zhang X 2017 Observation of acoustic Dirac-like cone and double zero refractive index *Nat. Commun.* **8** 14871
[41] Dubois M, Shi C, Wang Y and Zhang X 2017 A thin and conformal metasurface for illusion acoustics of rapidly changing profiles *Appl. Phys. Lett.* **110** 151902
[42] Schurig D, Mock J J, Justice B J, Cummer S A, Pendry J B, Starr A F and Smith D R 2006 Metamaterial electromagnetic cloak at microwave frequencies *Science* **314** 977–80
[43] Li J and Pendry J B 2008 Hiding under the carpet: a new strategy for cloaking *Phys. Rev. Lett.* **110** 203901
[44] Valentine J, Li J, Zentgraf T, Bartal G and Zhang X 2009 An optical cloak made of dielectrics *Nat. Mater.* **8** 568–71
[45] Gharghi M, Gladden C, Zentgraf T, Liu Y, Yin X, Valentine J and Zhang X 2011 A carpet cloak for visible light *Nano Lett.* **11** 2825–8
[46] Zentgraf T, Valentine J, Tapia N, Li J and Zhang X 2010 An optical 'Janus' device for integrated photonics *Adv. Mater.* **22** 2561–4
[47] Liu Y, Zentgraf T, Bartal G and Zhang X 2010 Transformational plasmon optics *Nano Lett.* **10** 1991–7
[48] Zentgraf T, Liu Y, Mikkelsen M H, Valentine J and Zhang X 2011 Plasmonic Luneburg and Eaton lenses *Nat. Nanotechnol.* **6** 151–5
[49] Palomba S, Zhang S, Park Y, Bartal G, Yin X and Zhang X 2012 Optical negative refraction by four-wave mixing in thin metallic nanostructures *Nat. Mater.* **11** 34–8
[50] Pendry J B 2008 Time reversal and negative refraction *Science* **322** 71–3
[51] Suchowski H, O'Brien K, Wong Z J, Salandrino A, Yin X and Zhang X 2013 Phase mismatch-free nonlinear propagation in optical zero-index materials *Science* **342** 1223–6
[52] O'Brien K, Suchowski H, Rho J, Salandrino A, Kante B, Yin X and Zhang X 2015 Predicting nonlinear properties of metamaterials from the linear response *Nat. Mater.* **14** 379–83
[53] Yu N and Capasso F 2014 Flat optics with designer metasurfaces *Nat. Mater.* **13** 139–50
[54] Ni X, Wong Z J, Mrejen M, Wang Y and Zhang X 2015 An ultrathin invisibility skin cloak for visible light *Science* **349** 1310–4
[55] Hosten O and Kwiat P 2008 Observation of the spin Hall effect of light via weak measurements *Science* **319** 787–90
[56] Yin X, Ye Z, Rho J, Wang Y and Zhang X 2013 Photonic spin Hall effect at metasurfaces *Science* **339** 1405–7
[57] Zhang S, Ye Z, Wang Y, Park Y, Bartal G, Mrejen M, Yin X and Zhang X 2012 Anti-Hermitian plasmon coupling of an array of gold thin-film antennas for controlling light at the nanoscale *Phys. Rev. Lett.* **109** 193902
[58] Jha P K, Ni X, Wu C, Wang Y and Zhang X 2015 Metasurface-enabled remote quantum interference *Phys. Rev. Lett.* **115** 025501
[59] O'Brien K, Macklin C, Siddiqi I and Zhang X 2014 Resonant phase matching of Josephson junction traveling wave parametric amplifiers *Phys. Rev. Lett.* **113** 157001
[60] Macklin C, O'Brien K, Hover D, Schwartz M E, Bolkhovsky V, Zhang X, Oliver W D and Siddiqi I 2015 A near-quantum-limited Josephson traveling-wave parametric amplifier *Science* **350** 307–10
[61] Procopio L M, Rozema L A, Wong Z J, Hamel D R, O'Brien K, Zhang X, Dakic B and Walther P 2017 Single-photon test of hyper-complex quantum theories using a metamaterial *Nat. Commun.* **8** 15044
[62] Zhang S, Genov D A, Sun C and Zhang X 2008 Cloaking of matter waves *Phys. Rev. Lett.* **100** 123002
[63] Zhang S, Genov D A, Wang Y, Liu M and Zhang X 2008 Plasmon-induced transparency in metamaterials *Phys. Rev. Lett.* **101** 047401
[64] Guo A, Salamo G J, Duchesne D, Morandotti R, Volatier-Ravat M, Aimez V, Siviloglou G A and Christodoulides D N 2009 Observation of PT-symmetry breaking in complex optical potentials *Phys. Rev. Lett.* **103** 093902
[65] Feng L, Wong Z J, Ma R-M, Wang Y and Zhang X 2014 Single-mode laser by parity-time symmetry breaking *Science* **346** 972–5
[66] Wong Z J, Xu Y-L, Kim J, O'Brien K, Wang Y, Feng L and Zhang X 2016 Lasing and anti-lasing in a single cavity *Nat. Photon.* **10** 796–801